Article

Discovery Medicine 2025; 37(196): 871–883
https://doi.org/10.24976/Discov.Med.202537196.77

Investigating the Role of Ferroptosis in Soman-Induced Neurotoxicity: A Pathway to New Potential Therapeutic Targets

Xiaosa Yang[1,2], Jiahua Zhao[1], Yuheng Shan[2], Mengyao Wang[3,4], Xiaojiao Xu[1], Tiantian Zhuang[1], Jiatang Zhang[1,*,†], Zhiyong Nie[4,*,†]

[1]Department of Neurology, The First Medical Centre, Chinese PLA General Hospital, 100853 Beijing, China
[2]Department of Neurology, Characteristic Medical Centre of People's Armed Police Force, 300162 Tianjin, China
[3]School of Pharmacy, Henan University, 475004 Kaifeng, Henan, China
[4]State Key Laboratory of Toxicology and Medical Countermeasures, Laboratory of Toxicant Analysis, Academy of Military Medical Sciences, 100850 Beijing, China
*Correspondence: zjt1128@aliyun.com (Jiatang Zhang); niezhiyong2008@163.com (Zhiyong Nie)
†These authors contributed equally.
Published: 20 May 2025

Background: Soman is a highly toxic organophosphorus nerve agent that can cause persistent neurotoxicity. However, the mechanism of soman-induced neurotoxicity has not been completely clarified. Ferroptosis, a novel type of programmed cell death, has been confirmed to precipitate neurotoxicity caused by organophosphorus flame retardant. Since studies on the relationship between ferroptosis and soman-induced neurotoxicity are lacking, the purpose of this research is to explore the mechanism of soman-induced neurotoxicity from the perspective of ferroptosis.

Methods: Institute of Cancer Research (ICR) mice were injected subcutaneously with low-dose soman (1/2 × median lethal dose (LD_{50})) daily for seven consecutive days to evaluate the neurotoxic injury caused by soman through alterations in body weight, cholinesterase activity, and neuronal counting. The morphologic changes of neurons and levels of ferroptosis-related molecules, including glutamate, glutathione (GSH), system xc^- (xCT), glutathione peroxidase 4 (GPX4), and malondialdehyde (MDA), were evaluated to confirm the involvement of ferroptosis in soman-induced neurotoxicity. The ferroptosis inhibitor ferrostatin-1 (Fer-1, 5 mg/kg) was administered daily immediately following soman exposure to further explore the role of ferroptosis.

Results: Repeated exposure to low-dose soman caused weight loss and neuronal death, and reduced cholinesterase activity. Meanwhile, it induced morphological changes of neurons characteristic of ferroptosis, increased glutamate and MDA levels, decreased GSH, and downregulated xCT and GPX4. Conversely, Fer-1 treatment mitigated neurotoxic injury and reversed the changes in ferroptosis-related molecule levels.

Conclusion: These findings indicate that ferroptosis engages in the course of neurotoxicity caused by soman and exerts a harmful effect via the glutamate/xCT/GPX4 pathway. This study provides new potential therapeutic targets for countermeasures against soman exposure.

Keywords: soman; neurotoxicity; ferroptosis; glutamate; system xc^-; glutathione peroxidase 4

Introduction

Soman is a classical organophosphorus nerve agent associated with extremely high toxicity and rapid lethality. It was first synthesized accidentally during research on insecticide development and has been used in military conflicts and terrorist attacks since World War II [1]. Soman causes the aging of acetylcholinesterase (AChE) within minutes, contributing to a strong inhibition of AChE and failure of reactivation [2]. This gives rise to the accumulation of acetylcholine, which consequently leads to severe neurotoxic symptoms and mass mortality. Medical interventions that can effectively detoxify soman are scarce owing to the instant aging of soman-poisoning AChE [3]. Moreover, the acute toxic effects of soman continually threaten the organ function of survivors, particularly the nervous system. The increase of acetylcholine triggered by soman subsequently stimulates the excessive release of the excitatory neurotransmitter glutamate and the overactivation of glutamate receptors in the later phase [4]. Glutamate and its specific receptors mediate neuronal excitotoxicity, initiating and maintaining status epilepticus, which in turn leads to ischemic and hypoxic degeneration and neuronal death, especially in the hippocampus, amygdala, piriform, and cerebral cortex [5,6]. Additionally, glutamate receptors take part in long-term potentiation and synaptic plasticity

in hippocampal neurons, which are crucial for learning and memory functions [7]. Several studies have revealed that over-accumulation of glutamate and its receptors caused by chronic exposure to soman leads to recurrent epilepsy and cognitive impairment, and antagonists of glutamate and its receptors can alleviate these neurotoxic symptoms [8,9]. While it is recognized that glutamate engages in the sustained neurotoxic damage caused by soman, deeper mechanisms still need to be uncovered to identify potential therapeutic targets of soman-induced neurotoxicity and promote the medical prognosis and quality of life of survivors.

As a newly recognized form of programmed cell death, ferroptosis is marked by an excessive load of ferrous ions and a buildup of lipid peroxides [10]. The amino acid antioxidant system, which involves molecules such as glutamate, system xc^- (xCT), and glutathione peroxidase 4 (GPX4), has a major impact on ferroptosis [11]. xCT is a membrane protein that facilitates the entry of cystine into cells while simultaneously discharging glutamate, based on concentration gradients [12]. GPX4, belonging to the glutathione peroxidases (GPXs) family, converts lipid peroxides into non-toxic substances, with the assistance of glutathione (GSH) [13]. Under pathological conditions, the increasing glutamate interferes with xCT function and cystine absorption, directly affecting GSH synthesis from cysteine [14]. The resulting decrease in GSH greatly diminishes GPX4's antioxidant capacity to prevent the degradation of lipid peroxides into harmful products, including malondialdehyde (MDA) and 4-hydroxynonenal, eventually resulting in ferroptosis [15]. Pieces of evidence have illustrated that ferroptosis aggravates pathological progressions of neurological diseases, such as Alzheimer's and cerebrovascular diseases [16,17]. Moreover, research demonstrated that tris(1,3-dichloro-2-propyl) phosphate (TDCPP), a type of organophosphorus flame retardant, induces ferroptosis, causing cognitive impairment and neuronal death in mice. The use of the ferroptosis inhibitor ferrostatin-1 (Fer-1) relieves neurotoxic injury, indicating a strong connection between ferroptosis and TDCPP-induced neurotoxicity [18]. Given that ferroptosis is involved in the TDCPP-induced neurotoxicity and can be triggered by the increase of glutamate, it is plausible that ferroptosis may be attributed to the significant release of glutamate caused by the organophosphorus nerve agent soman and further contribute to neurotoxicity. However, studies on how ferroptosis contributes to soman-induced neurotoxicity are still insufficient.

Therefore, we speculated that ferroptosis might contribute to the pathology of soman-induced neurotoxic injury by involving the regulation of glutamate, xCT, and GPX4. By detecting neurotoxic reactions and the levels of glutamate, xCT, GPX4, and other molecules after soman exposure and Fer-1 intervention in mice, we intended to establish the connection between ferroptosis and soman-induced neurotoxicity.

Materials and Methods

Animals

A total of 102 healthy adult male Institute of Cancer Research (ICR) mice (each weighing 20–22 g) were purchased from Charles River (Beijing, China; License: SCXK (J) 2021–0011). Prior to experiments, the mice were housed in cages set under a natural day-night cycle for one week and given access to food and water *ad libitum*. The rearing ambient temperature and humidity were set to the range of 22–26 °C and 50%–70%, respectively.

Based on prior references, mice were given subcutaneous single injections of soman available in various concentrations and the survival rate within 24 h was recorded [19,20]. For ICR mice, the median lethal dose (LD_{50}) of soman was finally defined to be 130 µg/kg. Mice were subcutaneously administered with 1/2 × LD_{50} soman (65 µg/kg) once daily for 1, 3, 5, and 7 days (n = 9 per time point). An equal volume of saline was administered to the control mice in the same way. Body weight was recorded before each injection. The occurrence frequency and duration of poisoning symptoms, including salivation, local and general convulsions, ataxia, Straub tail, and respiratory depression, were noted within 30 min post-injection. Mice were euthanized by cervical dislocation 30 min after exposure at different time points, and subsequently, brain tissue samples and blood specimens from the heart were collected. The blood samples were collected into anticoagulant tubes and centrifuged to obtain plasma, which was stored at –80 °C for further analysis.

Based on the frequently used dosage of Fer-1 (HY-100579, MCE, South Brunswick, NJ, USA) for mice in the reagent instruction, as well as our preliminary experiments on dosage safety, we adjusted the Fer-1 dosage to 5 mg/kg. Fer-1 was diluted in saline containing dimethyl sulfoxide (DMSO), Polyethylene glycol 300 (PEG-300) (202371, Sigma-Aldrich, St. Louis, MO, USA), and Tween-80 before use. For the Fer-1 intervention experiments, mice were randomly split into the control, soman, and soman + Fer-1 groups, with six mice in each. In the soman + Fer-1 group, intraperitoneal Fer-1 (5 mg/kg) treatment was administered daily for seven consecutive days immediately after subcutaneous injection of soman set at 1/2 × LD_{50} (65 µg/kg). The soman group was administered an equal dose of soman without Fer-1, while the control group was given saline. Body weight and poisoning symptoms were documented as described earlier. All mice in the three groups were euthanized by cervical dislocation on day 7 to collect brain tissue and blood for subsequent use.

Safety Precautions for Soman Usage

Soman (purity >95%) was offered by the Institute of Chemical Defense of the Chinese People's Liberation Army (Beijing, China). Pure soman was stocked in propylene glycol at –20 °C and diluted with cold saline before use. The

diluted soman must be used up within 10 min to prevent degradation. Soman must be handled with caution in a fume hood by personnel who have received professional safety training and are familiar with emergency response protocols. To prevent exposure to skin or eyes, personal protective equipment, such as masks, gloves, and safety goggles, should be worn. Used materials must be disposed of appropriately and not casually discarded. Any remaining toxic solutions should be sealed and decontaminated in the designated containers.

Cholinesterase Activity Assay

The colorimetric method proposed by Ellman was employed to detect cholinesterase activity [21]. Brain tissues were homogenized using cold phosphate-buffered saline (PBS) containing 0.1% Triton X-100, and then centrifuged to obtain the supernatant. The assay was performed using a 96-well plate, with each group assayed in triplicate. 40 µL of diluted plasma or brain supernatant (1:10 diluted by PBS), or PBS for the blank group, was mixed with 20 µL of 5,5′-Dithiobis (2-nitrobenzoic acid) (DTNB) (final concentration 0.3 mM, D8130, Sigma-Aldrich, St. Louis, MO, USA), followed by incubation at 37 °C for 10 min. Then, 20 µL of acetylcholine (final concentration 0.45 mM, A5751, Sigma-Aldrich, St. Louis, MO, USA) and 120 µL of PBS were added to all wells. Absorbance at 412 nm was continuously monitored with the Infinite M1000 Pro microplate reader (Tecan, Männedorf, Switzerland) at 37 °C for 20 times at 1-min intervals. The enzyme activity was determined using the formula provided below, where A represents the slope of the absorbance-time curve fitted by simple linear regression:

$$\text{Activity}(\%) = (A_{\text{sample}} - A_{\text{blank}}) / (A_{\text{control}} - A_{\text{blank}}) \times 100\%.$$

Nissl Staining and Transmission Electron Microscopy

Brain tissue was fixed and embedded in paraffin before sectioning. By standard conventions, these sections were dewaxed with water, incubated with Nissl staining solution (G1086, Servicebio, Wuhan, China), and then dehydrated and sealed. An ECLIPSE E100 light microscope (Nikon, Tokyo, Japan) was utilized to capture images for analysis. Five visual fields in the hippocampal Cornu Ammonis 1 (CA1) region were randomly selected for neuron counting.

Approximately 1 mm^3 of brain tissue was collected on ice, fixed in 2% glutaraldehyde (G1102, Servicebio, Wuhan, China), dehydrated, permeabilized, and embedded to prepare ultrathin sections, which were then incubated with uranyl acetate and lead citrate. An HT7700 electron microscope (HITACHI, Tokyo, Japan) was utilized to capture images for analysis.

HPLC Fluorescence Analysis

An Acquity Arc high-performance liquid chromatography (HPLC) equipped with a 2475 fluorescent detector (Waters, Milford, MA, USA) was utilized to measure the levels of glutamate and GSH in brain tissues. For sample pretreatment, brain tissues were homogenized and centrifuged at 4 °C to obtain supernatant for later use. The derivatization reagent was freshly produced by mixing 9 mg of o-phthalaldehyde (P108633, Aladdin, Shanghai, China), 167 µL of methanol (A452-4, ThermoFisher, Waltham, MA, USA), 1.5 mL of sodium tetraborate (0.2 M, S102367, Aladdin, Shanghai, China), and 18 µL of 2-mercaptoethanol (M301574, Aladdin, Shanghai, China). The sample was mixed thoroughly with the derivatization reagent in a 2:1 ratio. After reacting for 5 min, the mixture was injected into the liquid chromatograph for analysis. Glutamate (G1251, Sigma-Aldrich, St. Louis, MO, USA) and GSH (PHR1359, Sigma-Aldrich, St. Louis, MO, USA) standards were dissolved in deionized water at gradient concentrations and injected alongside brain samples to establish a standard curve. The content of glutamate and GSH in the brain tissue was expressed as µg/mg tissue.

A Waters Sunfire C18 reversed-phase column (4.6 × 150 mm, 5 µm, Waters, MA, USA) was utilized at 40 °C. The HPLC conditions and fluorescence parameters are as follows: mobile phase A (pH 5.8) consists of 90% sodium acetate aqueous solution (25 mM, S431678, Aladdin, Shanghai, China) and 10% methanol; and mobile phase B is acetonitrile (A998-4, ThermoFisher, Waltham, MA, USA). The target analytes were separated by isocratic elution with 85% mobile phase A and 15% mobile phase B and a 1 mL/min flow rate, with the sample plate kept at 4 °C. The entire process lasted 10 min, while the injection volume was 10 µL. The excitation wavelength and emission wavelength for the fluorescence detector were set at 340 nm and 450 nm, respectively.

MDA Assay

The MDA content in the samples was quantitated using an MDA assay kit (S0131S, Beyotime, Shanghai, China) in accordance with the manufacturer's instructions. Briefly, brain tissue was homogenized and centrifuged to obtain supernatant. Part of the supernatant was utilized for protein quantification using a Bicinchoninic Acid (BCA) assay kit (P0010, Beyotime, Shanghai, China), while the remaining supernatant was mixed with twice the volume of thiobarbituric acid (TBA) working solution containing antioxidants. The mixture was boiled for 15 min, cooled down, and centrifuged to obtain the supernatant. Absorbance at 532 nm was monitored with the Infinite M1000 Pro microplate reader (Tecan, Männedorf, Switzerland). The MDA content was determined by dividing the MDA assay results by the BCA quantified protein concentration, expressed as µmol/mg protein.

Western Blotting

Brain tissues were processed as described in the *MDA assay* section. Following protein quantification, the supernatant was subjected to sodium dodecyl-sulfate polyacrylamide gel electrophoresis (SDS-PAGE), and the bands were transferred onto a Polyvinylidene difluoride (PVDF) membrane (Millipore, Billerica, MA, USA). The PVDF membrane was blocked with 5% nonfat milk at ambient temperature for 2 h, followed by overnight incubation with the primary antibody (1:1000; ab307601 [xCT] and ab125066 [GPX4], Abcam, Cambridge, MA, USA; 4970 [β-actin], CST, Danvers, MA, USA) at 4 °C, and then a 2-h incubation with the secondary antibody (1:10,000, 7074, CST, Danvers, MA, USA) at ambient temperature. Ultimately, the PVDF membrane was treated with freshly prepared Enhanced chemiluminescence (ECL) solution and visualized using a FluorChem R imager (Protein Simple, San Jose, CA, USA). ImageJ software (Version 1.46r, National Institutes of Health, Bethesda, MD, USA) was utilized to measure the gray values of the protein bands for quantitative analysis of relative protein expression.

Immunofluorescence

Paraffin sections of mice brains were dewaxed with water, after which antigen recovery was performed. The sections were blocked for 1 h at ambient temperature, incubated with primary antibody (1:200; ab307601 [xCT] and ab125066 [GPX4] Abcam, Cambridge, MA, USA) overnight at 4 °C in a moist chamber, and then incubated with secondary antibody (1:200; ab6939 [goat anti-rabbit IgG H&L (Cy3) for xCT (red)], ab6717 [goat anti-rabbit IgG H&L (FITC) for GPX4 (green)], Abcam, Cambridge, MA, USA) coupled to a fluorescent dye for 1 h at ambient temperature in dark. After three washes, the sections were incubated with 4′,6-diamidino-2-phenylindole (DAPI, G1012, Servicebio, Shanghai, China) for 10 min at ambient temperature. An Eclipse C1 fluorescence microscope (Nikon, Tokyo, Japan) was utilized to capture images for fluorescence intensity analysis.

Statistical Analysis

Statistical analyses and graph illustrations were conducted using IBM SPSS Statistics software (Version 26.0, IBM Corp., Armonk, NY, USA) and GraphPad Prism software (Version 8.0, GraphPad Software, San Diego, CA, USA). Body weight measurements were repeated six times, while neuron counting was performed five times. All other experiments were carried out three times. The data are expressed as mean $\pm$ standard deviation (SD). The Shapiro–Wilk test was utilized to assess the normality of data distribution across all groups. A one-way analysis of variance (ANOVA) was used to analyze normally distributed data involving three or more groups. Dunnett's test was applied to identify differences between specific groups and the control group, and the Bonferroni test was used to assess differences between particular groups. For non-normally distributed data, the Kruskal–Wallis H test was employed. A two-way repeated measures ANOVA was used to analyze changes in body weight over time across two or more groups. Post hoc analyses were performed using the Bonferroni test to determine differences between specific groups. Statistical significance was defined as $p < 0.05$, with $p < 0.01$ and $p < 0.001$ indicating higher levels of significance.

Results

Repeated Exposure to Low-Dose Soman Induced Persistent Neurotoxic Reactions in Mice

To investigate whether repeated exposure to low-dose soman ($1/2 \times LD_{50}$) caused intoxication in mice, we recorded the body weight, poisoning symptoms, and cholinesterase activity. Upon the first exposure to soman, mice exhibited normal or mild symptoms within 30 min, including convulsions at the injection site and salivation. Starting from the second exposure, the mice exhibited deterioration of poisoning symptoms in a gradual fashion, which progressed from local limb convulsions and respiratory rhythm disorder to general convulsions, ataxia, Straub tail, and respiratory depression. Besides, the body weight of mice in the soman group was significantly lower than that of the control group from days 3 to 7 ($p < 0.001$, Fig. 1A). In addition, plasma and brain cholinesterase activities in the soman group decreased significantly on days 1, 3, 5, and 7 when compared to the control group ($p < 0.001$, Fig. 1B,C). These results revealed that repeated exposure to $1/2 \times LD_{50}$ soman suppressed the growth and induced neurotoxic reactions in mice.

Repeated Exposure to Low-Dose Soman Damaged Hippocampal Neurons in Mice

The structural changes in hippocampal neurons caused by soman exposure were assessed by Nissl staining and transmission electron microscopy. As shown in Fig. 2A, the hippocampal neurons in the granule cell layer were orderly arranged, showing distinct cell boundaries and normally stained Nissl bodies in the control group. At the initial exposure to soman, the shape of neurons was similar to that in the control group. However, as the number of soman exposures increased, morphological changes in neurons became more pronounced, including cell swelling, disordered arrangement, unclear boundaries, and lighter-stained Nissl bodies, especially at the seventh exposure. Consistent with the trends of these morphological changes, the number of hippocampal neurons in the soman group did not differ from that in the control group on day 1 ($p > 0.05$) but significantly decreased on days 3, 5, and 7 ($p < 0.001$, Fig. 2B). The main alterations in subcellular morphology between the control and soman groups were mainly detected in the mitochondria (Fig. 2C). The mitochondria of normal neurons

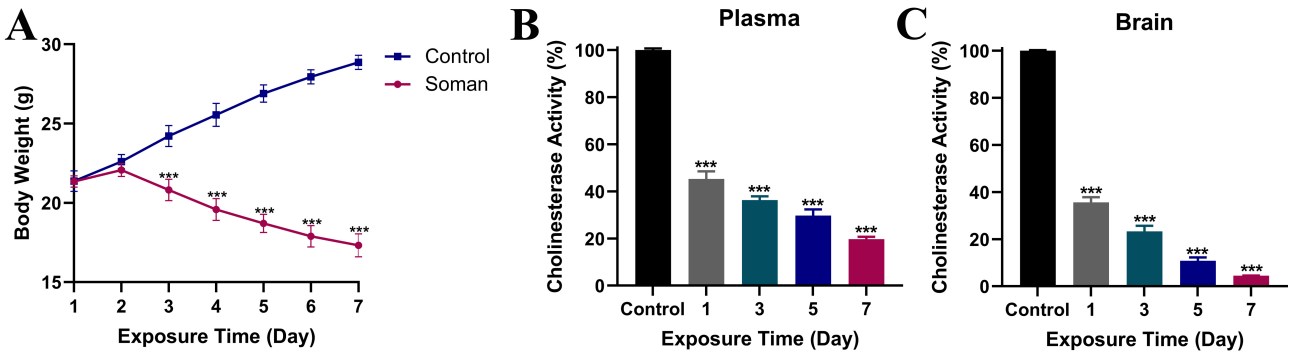

Fig. 1. Repeated exposure to low-dose soman (1/2 × LD_{50}) exerted persistent neurotoxic effects in mice. (A) The body weight of mice was recorded before the daily intoxication (n = 6 per group). The activity of cholinesterase in the plasma (B) and brain (C) was measured after different durations of soman exposure (*i.e.*, days) (n = 3 per time point). The cholinesterase activity (%) was calculated using the formula described in the Methods section, representing the proportion of cholinesterase activity in the experimental group to that in the control group. Data are presented as mean ± standard deviation (SD). *** $p < 0.001$ versus Control. LD_{50}, median lethal dose.

were elongated and elliptical in shape, with neatly arranged cristae and clear membrane contours. In contrast, the neuronal mitochondria of mice exposed to repeated low doses of soman shriveled to round or short rod-shaped and centrally vacuolized, with obviously reduced cristae and ruptured outer membranes. Almost no structural changes were detected in the cell nuclei of the control and soman groups under low magnification. These results indicated that repeated low-dose soman exposure damaged the structure and reduced the number of hippocampal neurons in mice.

Repeated Low-Dose Soman Exposure Induced Ferroptosis in Mice

To investigate whether ferroptosis occurred during repeated soman exposure, we examined the levels and expression of ferroptosis-associated indicators, including glutamate, GSH, MDA, xCT, and GPX4. There was no difference in brain glutamate levels between the control and soman groups on day 1 ($p > 0.05$). However, the glutamate levels in the soman group were significantly higher than those in the control group on days 3, 5, and 7 ($p < 0.001$, Fig. 3A,B). Additionally, the GSH levels in the soman group showed no differences on days 1 and 3 ($p > 0.05$) but significantly decreased on days 5 and 7 compared to the control group ($p < 0.001$, Fig. 3A,C). The level of MDA in the soman group was positively correlated with the duration of soman exposure, changing in tandem with glutamate levels. Except for day 1 ($p > 0.05$), the MDA level in the soman group significantly increased on day 3 ($p < 0.05$), day 5 ($p < 0.01$), and day 7 ($p < 0.001$) compared to the control group (Fig. 3D).

Western blotting results revealed that xCT and GPX4 presented a similar trend of relative expression over time. No significant differences in the expression of xCT and GPX4 were observed between the control and soman groups on days 1 and 3 ($p > 0.05$). However, significant downregulation was detected on days 5 and 7 compared to the control group ($p < 0.001$, Fig. 3E–G). Immunofluorescence results suggested that compared to the control group, the fluorescence intensity of xCT in the soman group showed no obvious changes on days 1 and 3 ($p > 0.05$) but significantly decreased on days 5 and 7 ($p < 0.001$, Fig. 3H,I). There was no significant difference in the fluorescence intensity of GPX4 between the control and soman groups on day 1 ($p > 0.05$). However, the fluorescence intensity of GPX4 in the soman group significantly decreased on day 3 ($p < 0.01$), day 5 ($p < 0.001$), and day 7 ($p < 0.001$) compared to the control group (Fig. 3J,K). The above results demonstrated that repeated low-dose soman exposure triggered ferroptosis in mice.

Ferroptosis Inhibitor Fer-1 Ameliorated the Neurotoxicity Caused by Soman in Mice

To evaluate the impact of Fer-1 on soman-induced neurotoxic injury, we recorded the poisoning symptoms and body weights of the mice while conducting cholinesterase activity assays and Nissl staining. Symptoms such as convulsions, ataxia, and respiratory depression caused by soman exposure were alleviated with Fer-1 intervention. The poisoning symptoms of mice in the soman + Fer-1 group at day 7 were comparable to those in the soman group on day 3. From days 3 to 7, the body weight of mice in the soman and soman + Fer-1 groups was significantly lower than that of the control group ($p < 0.01$ and $p < 0.001$). Of note, mice in the soman + Fer-1 group exhibited higher body weight compared to those in the soman group from days 4 to 7 ($p < 0.001$, Fig. 4A). Plasma and brain cholinesterase activities were significantly reduced in the soman and soman + Fer-1 groups compared to the control group ($p < 0.001$). Notably, the soman + Fer-1 group showed significant increases in both plasma and brain cholinesterase activities relative to the soman group ($p < 0.01$ and $p < 0.05$,

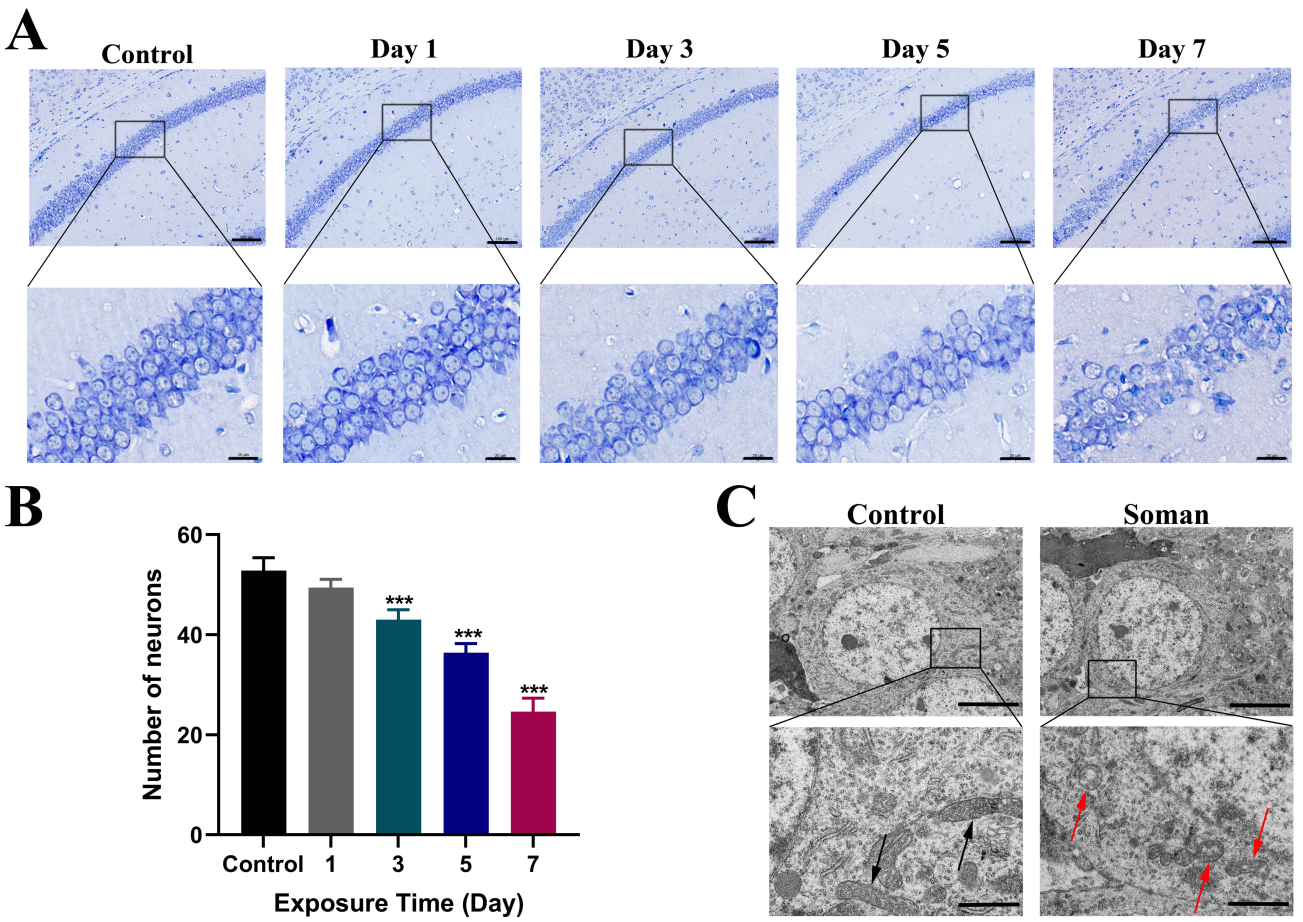

Fig. 2. Repeated exposure to low-dose soman (1/2 × LD_{50}) caused neuronal damage in the hippocampus of mice. (A) Nissl staining illustrates the morphological changes of neurons in the hippocampus caused by soman exposure at different time points. Scale bar: 100 µm (upper row) and 20 µm (bottom row). (B) The number of neurons was determined by counting performed on five randomly selected fields in the Nissl-stained images. The number of neurons reflects the effect of repeated soman exposure on hippocampal neurons. *** $p < 0.001$ versus Control. (C) Transmission electron microscopy revealed subcellular structural alterations in hippocampal neurons after seven exposures to soman. Black arrows indicate normal mitochondria, while red arrows represent mitochondria with abnormal structures. Scale bar: 5 µm (upper row) and 1 µm (bottom row).

Fig. 4B). Nissl staining indicated that a slightly disordered cell arrangement, a few cells with indistinct boundaries, and a handful of faded Nissl bodies were observed in the hippocampal region of poisoned mice treated with Fer-1, whereas these abnormalities were more severe in the hippocampus of soman-exposed mice without receiving Fer-1 treatment (Fig. 4D). Cell counting revealed that the number of hippocampal neurons was significantly lower in the soman and soman + Fer-1 groups than in the control group ($p < 0.001$), and the neurons of the soman + Fer-1 group significantly outnumbered those of the soman group ($p < 0.001$, Fig. 4C). These results demonstrated that Fer-1 alleviated soman-induced neurotoxic responses in mice.

Ferroptosis Inhibitor Fer-1 Alleviated Soman-Induced Neurotoxicity by Regulating Ferroptosis-Related Molecules

Next, we examined ferroptosis-related indicators to determine how the ferroptosis inhibitor Fer-1 mitigated soman-induced neurotoxicity, further elucidating how ferroptosis contributed to soman-induced neurotoxicity. HPLC results indicated that the glutamate levels in the soman and soman + Fer-1 groups were much higher than those in the control group ($p < 0.001$ and $p < 0.01$). The glutamate level in the soman + Fer-1 group significantly decreased compared to the soman group ($p < 0.05$, Fig. 5A,B). In contrast, the GSH levels in the soman and soman + Fer-1 groups were significantly lower than in the control group ($p < 0.001$ and $p < 0.01$). Notably, the soman + Fer-1 group exhibited a significantly higher GSH level compared to the soman group ($p < 0.001$, Fig. 5A,B). Regarding MDA levels in mice brains, the soman group showed a significant

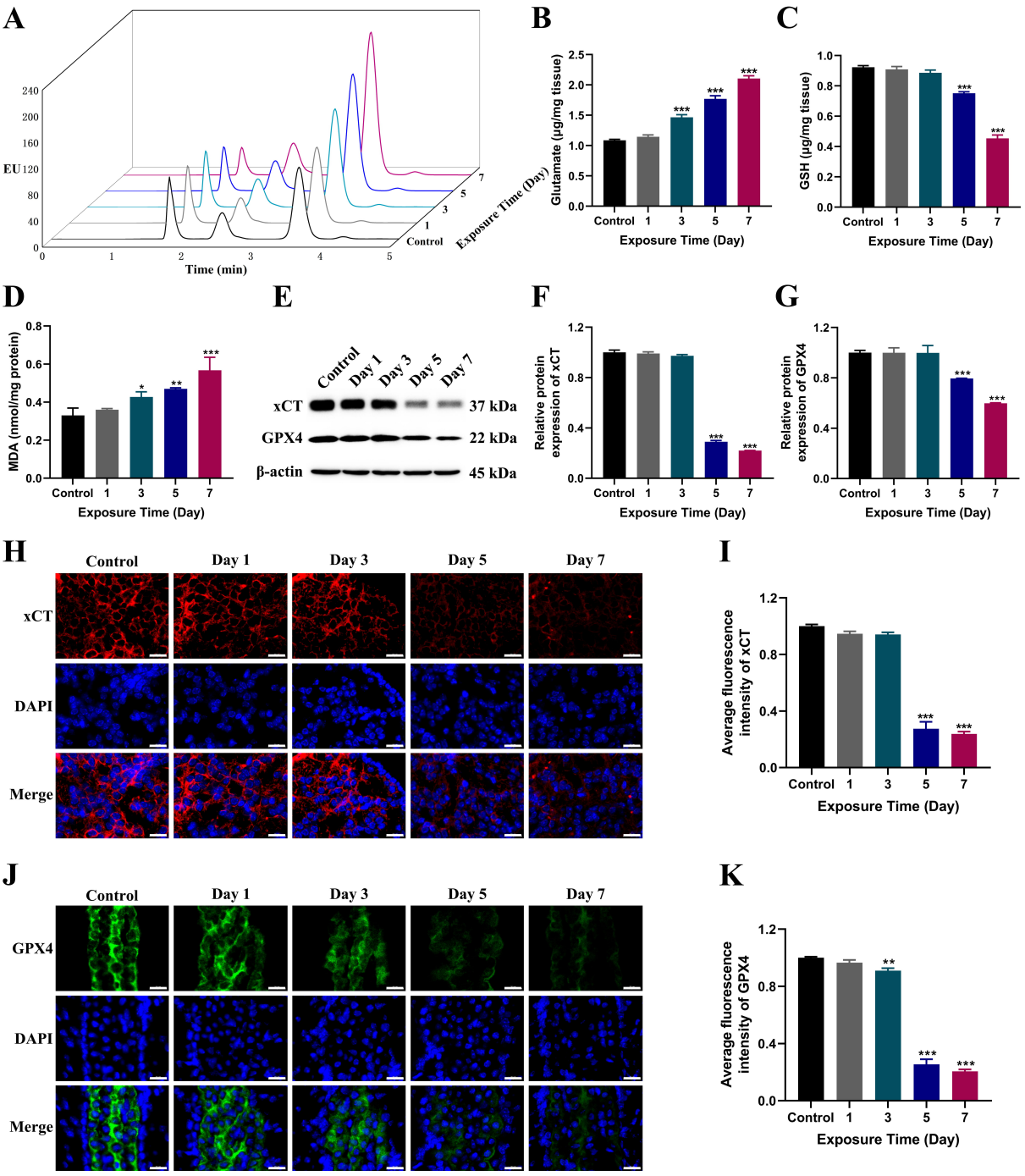

Fig. 3. Repeated exposure of low-dose soman (1/2 × LD_{50}) induced ferroptosis in mice (n = 3 per time point). (A–C) HPLC fluorescence detection was used to evaluate the effects of repeated soman exposure on glutamate and GSH levels in mice's brains. (A) The HPLC chromatogram shows that the retention times of GSH and glutamate were 1.70 and 3.57 min, respectively. The glutamate (B) and GSH (C) contents at different time points were determined using corresponding standard curves. Data are presented as mean ± SD. (D) The MDA level in mice's brains was measured at different time points of repeated soman exposure. (E–G) Changes in the relative expression of xCT and GPX4 caused by soman were measured by Western blotting. (E) The Western blotting for the bands of xCT and GPX4, with β-actin as the internal reference. The gray values of xCT (F) and GPX4 (G) were analyzed using ImageJ software. (H–K) Immunofluorescence results further confirm the effects of soman on the expression of xCT and GPX4. The immunofluorescence staining of xCT (H) and GPX4 (J), where xCT was stained in red, GPX4 in green, and nuclei in blue. Scale bar: 20 μm. Quantitative analysis of fluorescence intensity of xCT (I) and GPX4 (K). * $p < 0.05$, ** $p < 0.01$ and *** $p < 0.001$ versus Control. Abbreviations: GPX4, glutathione peroxidase 4; GSH, glutathione; HPLC, high-performance liquid chromatography; MDA, malondialdehyde; xCT, system xc^-.

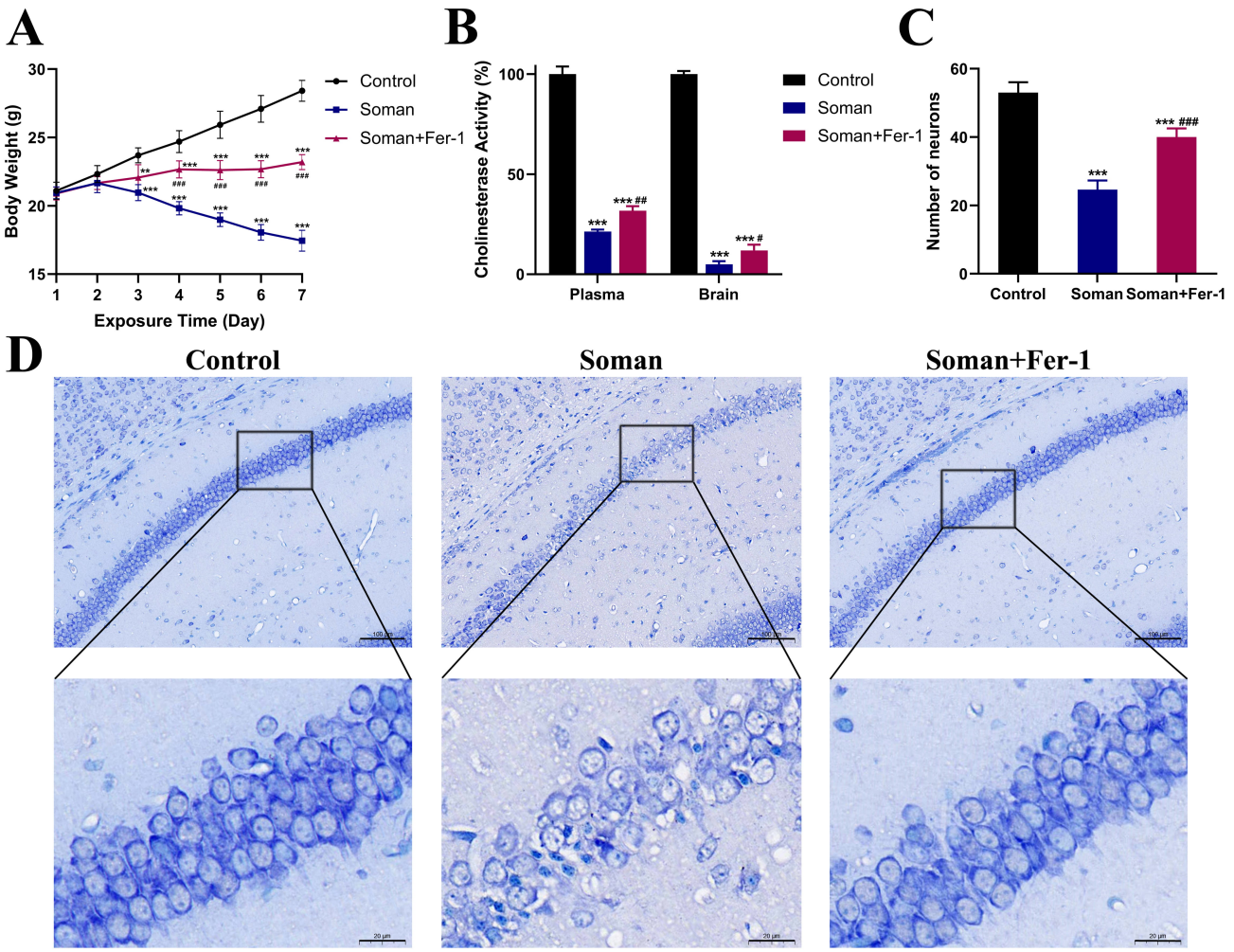

Fig. 4. The ferroptosis inhibitor Fer-1 alleviated the neurotoxic injury caused by soman in mice. (A) Body weight trends were recorded daily before drug administration ($n = 6$ per group). (B) Cholinesterase activity in the plasma and brain of mice was measured at the seventh exposure to soman (day 7) with and without Fer-1 ($n = 3$ per group). Data are presented as mean ± SD. (C) Comparison of the number of hippocampal neurons in intoxicated mice with and without Fer-1 treatment. (D) Nissl staining illustrates the protective effects of Fer-1 on morphological injury in hippocampal neurons caused by seven exposures to soman. Scale bar: 100 µm (upper row) and 20 µm (bottom row). ** $p < 0.01$ and *** $p < 0.001$ versus Control; $^{\#}$ $p < 0.05$, $^{\#\#}$ $p < 0.01$ and $^{\#\#\#}$ $p < 0.001$ versus Soman. Abbreviations: Fer-1, ferrostatin-1.

increase relative to the control group ($p < 0.01$). However, no significant difference was observed between the soman + Fer-1 and control groups ($p > 0.05$). Interestingly, the soman + Fer-1 group demonstrated a significant decrease in MDA level relative to the soman group ($p < 0.05$, Fig. 5C). Western blotting results suggested that the protein expression of xCT and GPX4 was significantly lower in the soman and soman + Fer-1 groups than in the control group ($p < 0.001$). However, a significant upregulation of xCT and GPX4 was detected in the soman + Fer-1 group compared to the soman group ($p < 0.001$, Fig. 5D,E). These findings were further supported by the immunofluorescence analysis, which indicated that the fluorescence intensity of xCT and GPX4 was significantly lower in the soman and soman + Fer-1 groups than in the control group ($p < 0.001$ and $p < 0.05$, respectively). Surprisingly, the fluorescence intensity of xCT and GPX4 significantly increased in the soman + Fer-1 group compared to the soman group ($p < 0.001$, Fig. 5F–H). These results implied that Fer-1 modulated ferroptosis-related molecules to attenuate the neurotoxicity caused by soman.

Discussion

The aim of the current study was to explore if ferroptosis contributes to soman-induced neurotoxicity, a topic that has not been fully explored. Our results revealed that repeated low-dose exposure to soman leads to neurotoxic responses, including decreased body weight, inhibition of cholinesterase activity, and reduced numbers of neurons. Furthermore, we observed characteristic alterations associ-

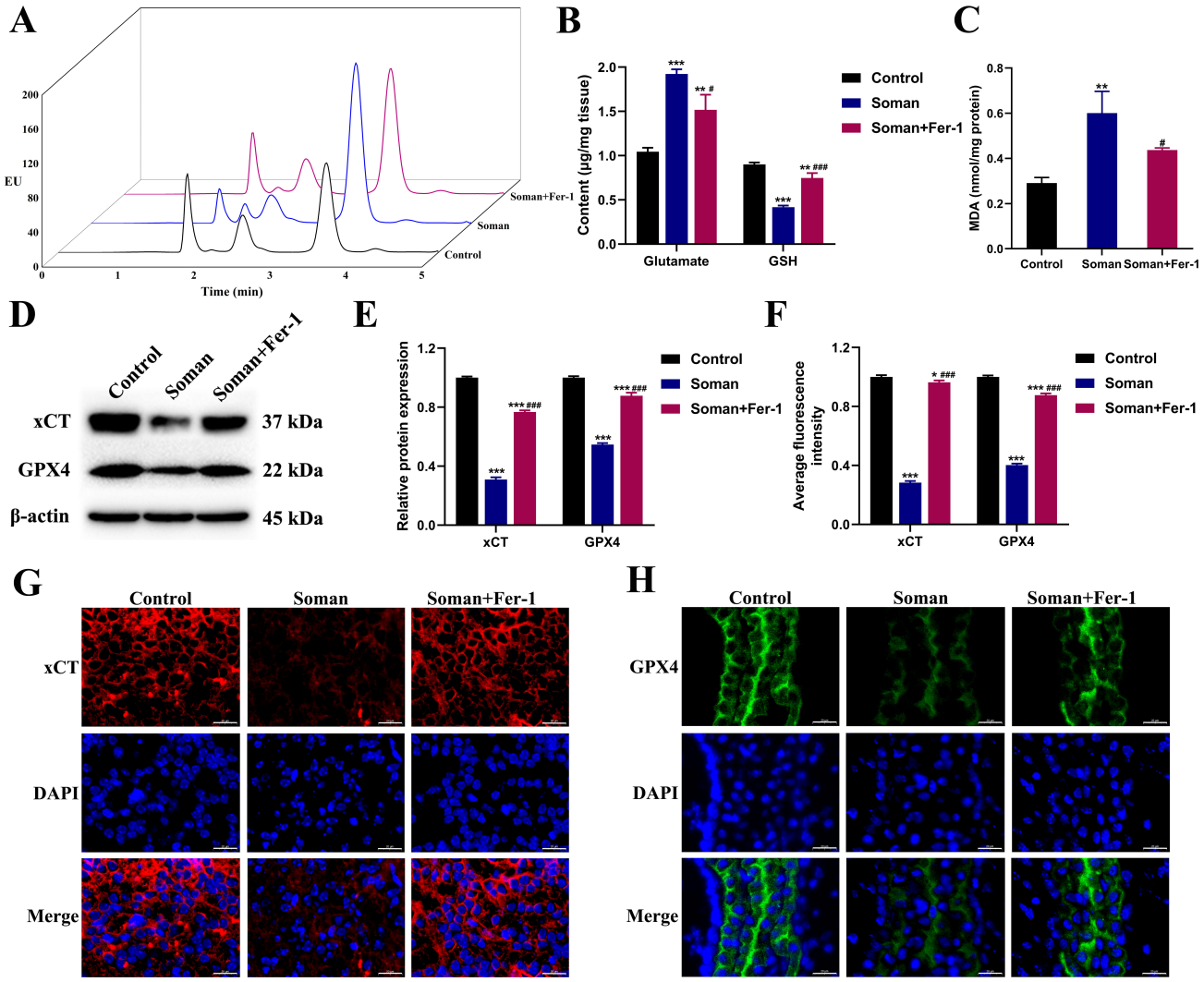

Fig. 5. The ferroptosis inhibitor Fer-1 reversed the alterations in ferroptosis-related molecule levels caused by soman in mice (*n* = 3 per group). (A) HPLC chromatograms showing the retention times of GSH and glutamate at 1.70 and 3.57 min, respectively. (B) Comparison of glutamate and GSH levels in the brains of intoxicated mice with and without Fer-1 intervention. Data are presented as mean ± SD. (C) MDA level in the brain of soman-exposed mice with and without Fer-1 intervention. (D,E) Relative expression of xCT and GPX4 in the brains of intoxicated mice with and without Fer-1 intervention. (D) Western blotting showing the bands of xCT and GPX4, with β-actin acting as an internal reference. (E) Analysis of the gray values of xCT and GPX4. (F–H) Immunofluorescence-based validation of the effects of Fer-1 on the downregulation of xCT and GPX4 caused by soman. (F) Fluorescence intensity analysis of xCT and GPX4. * $p < 0.05$, ** $p < 0.01$ and *** $p < 0.001$ versus Control; $^{\#}$ $p < 0.05$ and $^{\#\#\#}$ $p < 0.001$ versus Soman. (G,H) Immunofluorescence staining of xCT (G) and GPX4 (H) where xCT was stained in red, GPX4 in green, and nuclei in blue. Scale bar: 20 μm.

ated with ferroptosis, including morphological changes in the mitochondria, increased glutamate and MDA, decreased GSH, and downregulated xCT and GPX4 in the mice's brains over time. Notably, these ferroptosis-associated changes in morphology and molecular levels could be reversed by a classic ferroptosis inhibitor, Fer-1. Our findings elucidate that ferroptosis is implicated in the progression of soman-induced neurotoxicity.

Soman exposure can lead to severe acute toxic symptoms and a series of long-term neurological sequelae. It has been reported that 74% of victims experienced neurological symptoms between 14 to 24 years after exposure to nerve agents. These symptoms included emotional regulation disorders, ataxia, cognitive impairment, motor disorders, dysarthria, and headaches, which severely affect the quality of life of survivors and even lead to a loss of self-care abilities [22]. Therefore, exploring the pathological mechanism of persistent neurotoxicity caused by soman exposure is vital for promoting the medical prognosis and quality of life of survivors. In our study, we aimed to mimic

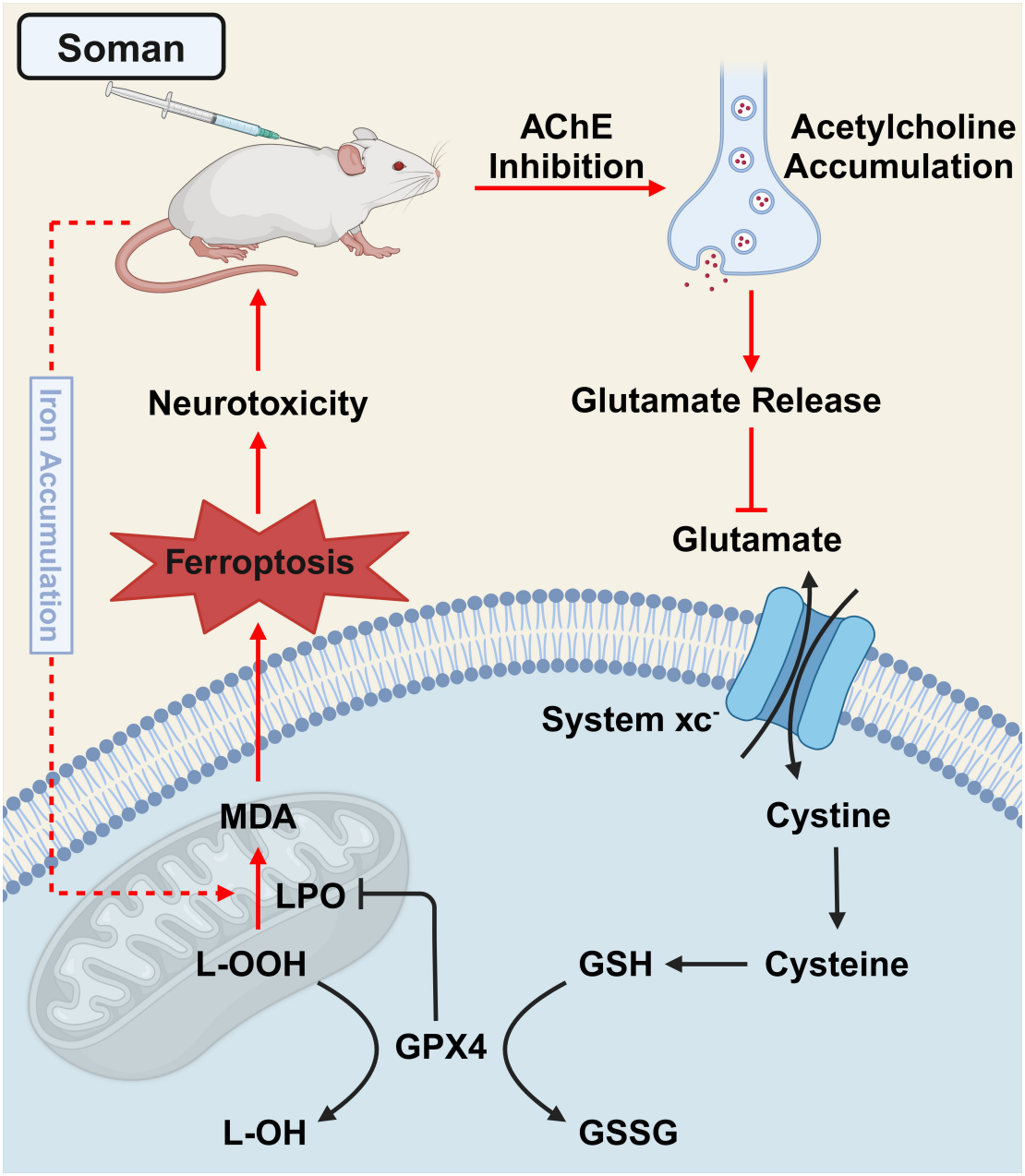

Fig. 6. Ferroptosis is involved in soman-induced neurotoxicity. Under normal physiological conditions (indicated by black arrows), system xc^- takes up extracellular cystine and exports intracellular glutamate. This process is auto-initiated by the substantial glutamate concentration gradient across compartments inside and outside the cells and does not require adenosine triphosphate (ATP). Once entering the cells, cystine is quickly reduced to cysteine, which then synthesizes GSH. GSH assists GPX4 in reducing toxic lipid peroxides (L-OOH) to nontoxic lipid alcohols (L-OH), thereby protecting neurons from damage. However, as indicated by red arrows, soman exposure inhibits AChE and leads to the accumulation of acetylcholine, which in turn results in the sustained release of glutamate. The increase in glutamate causes a decrease in cystine uptake and a consequent reduction in GSH synthesis. In the absence of adequate GSH, GPX4 cannot effectively prevent lipid peroxidation, a process that allows massive lipid peroxides to degrade into harmful products such as MDA. As a result, ferroptosis occurs and plays a vicious role in the pathological process of neurotoxic injury caused by soman. Abbreviations: AChE, acetylcholinesterase; GSSG, oxidized glutathione; LPO, lipid peroxidation. This figure was created with BioRender (https://www.Biorender.com).

the persistent neurotoxic injury caused by soman through repeated subcutaneous administration of lower-dose soman ($1/2 \times LD_{50}$) for seven days. The results indicated that this poisoning method led to severe and sustained poisoning symptoms and growth inhibition, as well as remarkable cholinesterase inhibition and neuronal injury. It has been

confirmed that soman stimulates the continuous release of the excitatory neurotransmitter glutamate and activates glutamate receptors on postsynaptic membranes, leading to excitotoxic nerve damage and resulting in recurrent epilepsy and cognitive impairment [23]. Consistently, our results showed that glutamate levels in the mice's brains gradually increased with the duration of soman exposure, paralleling the worsening neurotoxic reactions. The similar levels of glutamate in the control and soman groups at the first soman exposure were possibly since the glutamate levels increased following cholinergic system dysfunction and did not spike at the first exposure. Thus, it is evident that the neurotransmitter glutamate is vital for the pathological processes of soman-induced neurotoxicity.

Ferroptosis is a form of programmed cell death that differs from classical apoptosis and pyroptosis [24]. The morphological changes attributed to ferroptosis primarily occur in mitochondria, including organelle shrinkage, cristae reduction or disappearance, increased membrane density, and even membrane rupture. In contrast, the changes in nuclei are minimal [25]. Ferroptosis was influenced by the imbalance in the amino acid antioxidant system, lipid metabolism disorder, and other mechanisms, with the amino acid antioxidant system playing a crucial role, where glutamate acts as the upstream molecule [26]. A previous study has shown that glutamate suppressed neuroblastoma cell growth and induced ferroptosis by increasing MDA levels while reducing GSH and GPX4 levels, and Fer-1 administration reversed the alterations in the levels of ferroptosis-related molecules and mitigated the cellular neurotoxicity induced by glutamate [27]. Additionally, evidence suggested that the suppression of cerebral ferroptosis by Fer-1 treatment, through suppressing xCT and glutamate receptor, alleviated glutamate-mediated excitotoxicity and neuronal death, eventually improving the functional prognosis of mice with sepsis-associated encephalopathy [28]. Therefore, it can be argued that a surge in glutamate triggers ferroptosis and the activities of xCT and GPX4 considerably influence the occurrence of ferroptosis.

In this study, repeated exposure to low-dose soman led to changes in the morphological structure of neurons and the ferroptosis-related molecules, which occurred simultaneously with neurotoxic injury in the tested mice. Notably, the morphological changes observed in the neuronal mitochondria caused by soman exposure closely resembled the characteristics of ferroptosis. Additionally, soman exposure led to an increase in glutamate level, which downregulated xCT. This downregulation subsequently decreased the GSH level, weakened the relative expression of GPX4, and resulted in a significant increase in MDA in mice brains. Since xCT, GSH, and GPX4 are the downstream molecules of glutamate, as mentioned above, it is likely that their decline occurred following the rise in glutamate. Interestingly, the increase in MDA occurred prior to the changes in GSH, GPX4, and xCT. One possible explanation for this phenomenon is that iron accumulation resulting from soman exposure, another pathway related to ferroptosis, also enhanced lipid peroxidation [29]. The combined effects of iron accumulation and glutamate release likely contributed to the earlier increase in MDA. Furthermore, our results indicated that the ferroptosis inhibitor Fer-1 alleviated toxic effects and neuronal death, reduced levels of glutamate and MDA, increased GSH content, and upregulated xCT and GPX4, a finding consistent with previous studies on organophosphorus and ferroptosis [18,30]. Our findings illustrate a plausible pathway in which repeated exposure to low-dose soman increases glutamate, which further downregulates xCT and GPX4, ultimately triggering ferroptosis and contributing to the pathological mechanism of soman-induced neurotoxicity (Fig. 6). In other words, ferroptosis is involved in soman-induced neurotoxicity via the glutamate/xCT/GPX4 pathway. At present, no effective medication is available for instantly resolving soman intoxication because AChE can be aged by soman within minutes [2]. Thus, investigations on the role of ferroptosis and the development of effective antagonists against ferroptosis are warranted so as to provide a new therapeutic strategy for reducing neurotoxicity and increasing survival rate after soman exposure.

Although we clarified that ferroptosis is implicated in the soman-induced neurotoxicity through the dysfunction of the amino acid antioxidant system, other signaling pathways associated with ferroptosis, including iron metabolism disorders, lipid metabolic abnormalities, and ferritin-related autophagy, need to be examined to further elucidate the relationship between ferroptosis and soman. Additionally, monotherapy for soman intoxication often has limited efficacy. Therefore, it is necessary to evaluate the effects of combination therapy using ferroptosis inhibitors and drugs targeting other mechanisms to better alleviate the neurotoxicity caused by soman.

Conclusion

By assessing neurotoxic damage, morphological changes, and alterations in the levels of ferroptosis-related molecules following repeated exposure to low-dose soman, this study demonstrates that ferroptosis participates in the pathogenesis of soman-induced neurotoxicity by mediating the glutamate/xCT/GPX4 pathway. This is the first research to elucidate the neurotoxic mechanism of soman from the perspective of ferroptosis, offering a novel potential target for further exploring soman-induced neurotoxicity and improving countermeasures against toxicity following soman exposures.

Availability of Data and Materials

The data are available from the corresponding authors upon reasonable request.

Author Contributions

XSY: Methodology, Formal analysis, Investigation, Writing—original draft, Writing—critical revision and editing. JHZ: Methodology, Validation, Investigation, Writing—original draft. YHS: Formal analysis, Writing—critical revision and editing. MYW: Methodology, Validation, Writing—critical revision and editing. XJX: Formal analysis, Writing—critical revision and editing. TTZ: Methodology, Writing—critical revision and editing. JTZ: Conceptualization, Writing—critical revision and editing, Supervision, Project administration. ZYN: Conceptualization, Resources, Writing—critical revision and editing. All authors have read and approved the final manuscript. All authors have participated sufficiently in the work and agreed to be accountable for all aspects of the work.

Ethics Approval and Consent to Participate

The Institutional Animal Care and Use Committee of National Beijing Center for Drug Safety Evaluation and Research evaluated and authorized all protocols concerning animal care and use (No. IACUC-2024-002B).

Acknowledgment

Not applicable.

Funding

This research received no external funding.

Conflict of Interest

The authors declare no conflict of interest.

References

[1] McCarren HS, McDonough JH, Jr. Anticonvulsant discovery through animal models of status epilepticus induced by organophosphorus nerve agents and pesticides. Annals of the New York Academy of Sciences. 2016; 1374: 144–150. https://doi.org/10.1111/nyas.13092.

[2] Sirin GS, Zhou Y, Lior-Hoffmann L, Wang S, Zhang Y. Aging mechanism of soman inhibited acetylcholinesterase. The Journal of Physical Chemistry. B. 2012; 116: 12199–12207. https://doi.org/10.1021/jp307790v.

[3] Figueiredo TH, Aroniadou-Anderjaska V, Pidoplichko VI, Apland JP, Braga MFM. Antiseizure and Neuroprotective Efficacy of Midazolam in Comparison with Tezampanel (LY293558) against Soman-Induced Status Epilepticus. Toxics. 2022; 10: 409. https://doi.org/10.3390/toxics10080409.

[4] Acon-Chen C, Koenig JA, Smith GR, Truitt AR, Thomas TP, Shih TM. Evaluation of acetylcholine, seizure activity and neuropathology following high-dose nerve agent exposure and delayed neuroprotective treatment drugs in freely moving rats. Toxicology Mechanisms and Methods. 2016; 26: 378–388. https://doi.org/10.1080/15376516.2016.1197992.

[5] Niquet J, Nguyen D, de Araujo Furtado M, Lumley L. Treatment of cholinergic-induced status epilepticus with polytherapy targeting GABA and glutamate receptors. Epilepsia Open. 2023; 8: S117–S140. https://doi.org/10.1002/epi4.12713.

[6] Yang XK, Tang Y, Qiu QF, Wu WT, Zhang FL, Liu YL, *et al*. Aβ_{1-42} Oligomers Induced a Short-Term Increase of Glutamate Release Prior to Its Depletion As Measured by Amperometry on Single Varicosities. Analytical Chemistry. 2019; 91: 15123–15129. https://doi.org/10.1021/acs.analchem.9b03826.

[7] Song Q, Li XH, Lu JS, Chen QY, Liu RH, Zhou SB, *et al*. Enhanced long-term potentiation in the anterior cingulate cortex of tree shrew. Philosophical Transactions of the Royal Society of London. Series B, Biological Sciences. 2024; 379: 20230240. https://doi.org/10.1098/rstb.2023.0240.

[8] Golime R, Singh N, Rajput A, Dp N, Lodhi VK. Chronic sub lethal nerve agent (Soman) exposure induced long-term neurobehavioral, histological, and biochemical alterations in rats. Journal of Chemical Neuroanatomy. 2024; 136: 102388. https://doi.org/10.1016/j.jchemneu.2024.102388.

[9] Joosen MJA, Jousma E, van den Boom TM, Kuijpers WC, Smit AB, Lucassen PJ, *et al*. Long-term cognitive deficits accompanied by reduced neurogenesis after soman poisoning. Neurotoxicology. 2009; 30: 72–80. https://doi.org/10.1016/j.neuro.2008.11.010.

[10] Gao M, Jiang X. To eat or not to eat-the metabolic flavor of ferroptosis. Current Opinion in Cell Biology. 2018; 51: 58–64. https://doi.org/10.1016/j.ceb.2017.11.001.

[11] Miao Y, Chen Y, Xue F, Liu K, Zhu B, Gao J, *et al*. Contribution of ferroptosis and GPX4's dual functions to osteoarthritis progression. EBioMedicine. 2022; 76: 103847. https://doi.org/10.1016/j.ebiom.2022.103847.

[12] Allen AE, Sun Y, Wei F, Reid MA, Locasale JW. Nucleotide metabolism is linked to cysteine availability. The Journal of Biological Chemistry. 2023; 299: 103039. https://doi.org/10.1016/j.jbc.2023.103039.

[13] Xu K, Li K, He Y, Mao Y, Li X, Zhang L, *et al*. Engineered nanoplatform mediated gas therapy enhanced ferroptosis for tumor therapy *in vivo*. Bioactive Materials. 2024; 44: 488–500. https://doi.org/10.1016/j.bioactmat.2024.10.024.

[14] Miotto G, Rossetto M, Di Paolo ML, Orian L, Venerando R, Roveri A, *et al*. Insight into the mechanism of ferroptosis inhibition by ferrostatin-1. Redox Biology. 2020; 28: 101328. https://doi.org/10.1016/j.redox.2019.101328.

[15] Liu P, Feng Y, Li H, Chen X, Wang G, Xu S, *et al*. Ferrostatin-1 alleviates lipopolysaccharide-induced acute lung injury via inhibiting ferroptosis. Cellular & Molecular Biology Letters. 2020; 25: 10. https://doi.org/10.1186/s11658-020-00205-0.

[16] Fu C, Wu Y, Liu S, Luo C, Lu Y, Liu M, *et al*. Rehmannioside A improves cognitive impairment and alleviates ferroptosis via activating PI3K/AKT/Nrf2 and SLC7A11/GPX4 signaling pathway after ischemia. Journal of Ethnopharmacology. 2022; 289: 115021. https://doi.org/10.1016/j.jep.2022.115021.

[17] Lane DJR, Metselaar B, Greenough M, Bush AI, Ayton SJ. Ferroptosis and NRF2: an emerging battlefield in the neurodegeneration of Alzheimer's disease. Essays in Biochemistry. 2021; 65: 925–940. https://doi.org/10.1042/EBC20210017.

[18] Qian B, Jiang RJ, Song JL, Wang CQ. Organophosphorus flame retardant TDCPP induces neurotoxicity via mitophagy-related ferroptosis in vivo and in vitro. Chemosphere. 2022; 308: 136345. https://doi.org/10.1016/j.chemosphere.2022.136345.

[19] Betapudi V, Goswami R, Silayeva L, Doctor DM, Chilukuri N. Gene therapy delivering a paraoxonase 1 variant offers long-term prophylactic protection against nerve agents in mice. Science Translational Medicine. 2020; 12: eaay0356. https://doi.org/10.1126/scitranslmed.aay0356.

[20] Kovarik Z, Maček Hrvat N, Katalinić M, Sit RK, Paradyse A, Žunec S, *et al*. Catalytic Soman Scavenging by the Y337A/F338A Acetylcholinesterase Mutant Assisted with Novel Site-Directed Aldoximes. Chemical Research in Toxicol-

ogy. 2015; 28: 1036–1044. https://doi.org/10.1021/acs.chemrestox.5b00060.

[21] Ellman GL, Courtney KD, Andres V, Jr, Featherstone RM. A new and rapid colorimetric determination of acetylcholinesterase activity. Biochemical Pharmacology. 1961; 7: 88–95. https://doi.org/10.1016/0006-2952(61)90145-9.

[22] Figueiredo TH, Apland JP, Braga MFM, Marini AM. Acute and long-term consequences of exposure to organophosphate nerve agents in humans. Epilepsia. 2018; 59: 92–99. https://doi.org/10.1111/epi.14500.

[23] Wang S, He H, Long J, Sui X, Yang J, Lin G, *et al*. TRPV4 Regulates Soman-Induced Status Epilepticus and Secondary Brain Injury via NMDA Receptor and NLRP3 Inflammasome. Neuroscience Bulletin. 2021; 37: 905–920. https://doi.org/10.1007/s12264-021-00662-3.

[24] Newton K, Strasser A, Kayagaki N, Dixit VM. Cell death. Cell. 2024; 187: 235–256. https://doi.org/10.1016/j.cell.2023.11.044.

[25] Li J, Jia YC, Ding YX, Bai J, Cao F, Li F. The crosstalk between ferroptosis and mitochondrial dynamic regulatory networks. International Journal of Biological Sciences. 2023; 19: 2756–2771. https://doi.org/10.7150/ijbs.83348.

[26] Wan Y, Chen J, Li J, Chen Z, Wang Y, Li J, *et al*. Cu^0-based nanoparticles boost anti-tumor efficacy via synergy of cuproptosis and ferroptosis enhanced by cuproptosis-induced glutathione synthesis disorder. Colloids and Surfaces. B, Biointerfaces. 2025; 245: 114196. https://doi.org/10.1016/j.colsurfb.2024.114196.

[27] Chen Z, Wang F, Chen Z, Zheng N, Zhou Q, Xie L, *et al*. Decursin ameliorates neurotoxicity induced by glutamate through restraining ferroptosis by up-regulating FTH1 in SH-SY5Y neuroblastoma cells. Neuroscience. 2024; 559: 139–149. https://doi.org/10.1016/j.neuroscience.2024.08.035.

[28] Xie Z, Xu M, Xie J, Liu T, Xu X, Gao W, *et al*. Inhibition of Ferroptosis Attenuates Glutamate Excitotoxicity and Nuclear Autophagy in a CLP Septic Mouse Model. Shock. 2022; 57: 694–702. https://doi.org/10.1097/SHK.0000000000001893.

[29] Putra M, Vasanthi SS, Rao NS, Meyer C, Van Otterloo M, Thangi L, *et al*. Inhibiting Inducible Nitric Oxide Synthase with 1400W Reduces Soman (GD)-Induced Ferroptosis in Long-Term Epilepsy-Associated Neuropathology: Structural and Functional Magnetic Resonance Imaging Correlations with Neurobehavior and Brain Pathology. The Journal of Pharmacology and Experimental Therapeutics. 2024; 388: 724–738. https://doi.org/10.1124/jpet.123.001929.

[30] Zhang Q, Luo C, Li Z, Huang W, Zheng S, Liu C, *et al*. Astaxanthin activates the Nrf2/Keap1/HO-1 pathway to inhibit oxidative stress and ferroptosis, reducing triphenyl phosphate (TPhP)-induced neurodevelopmental toxicity. Ecotoxicology and Environmental Safety. 2024; 271: 115960. https://doi.org/10.1016/j.ecoenv.2024.115960.